LARGE WATER ICE AEROSOLS IN MARTIAN NORTH POLAR CLOUDS

M. T. Lemmon, *Texas A&M University, College Station, TX, USA (lemmon@tamu.edu).*

Introduction:

Water ice clouds on Mars are important due to their influence on the global water cycle [Smith, 2008]. Ice aerosols have a size-dependent influence on the downward transport of water vapor [Kahn 1990], and a significant size-dependent radiative impact on climate [Urrata and Toon, 2013]. Limb images have shown high-altitude hazes with typical ice sizes of r=0.15-6 μm [Kahn, 1990]. Thermal Emission Spectrometer (TES) observations have shown that ice hazes are bimodal, with Type 1 (r=1-2 μm, crystalline) and Type 2 (r=3-4 μm, amorphous) ice hazes identified [Clancy *et al.,* 2003]. At the Mars Phoenix Lander site (68°N), fall streaks seen in lidar data have been interpreted as indicating r=35 μm ice aerosols [Whiteway *et al*., 2009]. Simulations of cloud microphysics coupled with a boundary layer model suggest that 30-50 μm crystals form and are responsible for a downward transport of water vapor [Daerden *et al*., 2010]. Yet, observational reports of such large ice aerosols are otherwise absent from the literature.

Observations:

The Surface Stereo Imager (SSI) on the Phoenix Mars Lander was equipped with 8 neutral-density coated interference filters for solar imaging. Four wavelengths, 451, 671, 887, and 991 nm, were used for monitoring atmospheric particulates. Over the mission, many images of the Sun were taken at different times of day. The brightness of the Sun was measured for each image. A relative calibration such as that described by Smith and Lemmon [1999] was used to determine, for each image, what the extinction compared to top-of-atmosphere insolation was. Optical depths were determined following the Beer-Lambert law, $F = F_{TOA} \bullet e^{-\tau \bullet \eta}$, where F is the measured flux, F_{TOA} is the top-of-atmosphere flux, τ is the desired normal-incidence optical depth, and η is the airmass, or ratio of slant-path optical depth to normal optical depth.

Figure 1 shows the 451-nm optical depth from sol (or Martian solar day) 4 to 151 of the mission (L_S=78.5-148.5°). Values for other wavelengths are similar. During the first 40 sols, the sky was relatively dusty. After sol 130, dust storms returned. Beginning about sol 70, ice clouds were occasionally observed; they were common after sol 100 [Moores et al., 2010]. Ice clouds show up in the opacity data as spikes of the same magnitude in each of the 4 filters.

An important aspect of the present investigation is that the extinction values were determined from resolved images of the Sun. Each flux determination was made after background removal, so forward-scattered light is correctly seen as extinction.

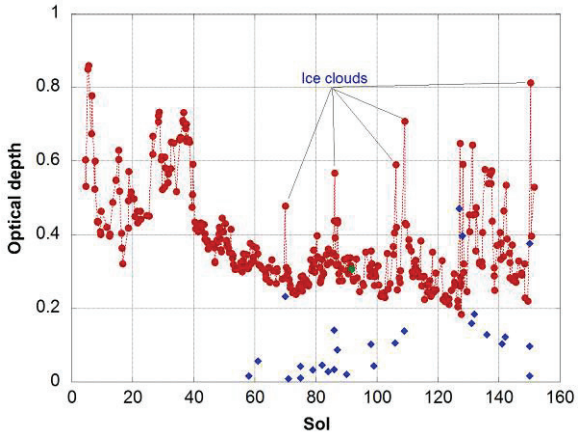

Figure 1. 451-nm atmospheric optical depth. Red values show total extinction optical depth. Blue values for some measurements show that part of the optical depth attributed to large ice aerosols (see text).

On several occasions, the optical depth spiked 0.2 or more above nearby measurements. This was seen in each filter. Inspection of the images showed that these had a bright region around the Sun that was distinctive from other images. A selection of such images is shown in Fig. 2. All images prior to sol 58 looked like the 'null' images in rows 2 and 5. Images similar to those in rows 1 and 4 were seen sporadically from sol 58 (L_S=130°) through the end of mission. The near-Sun scattered light is not an instrumental effect: (1) the effect is absent from most images of the mission; (2) images without the effect exist for similar geometries as those with the effect; (3) for sol 101, the effect is seen in images with the Sun partially behind a low hill to the north.

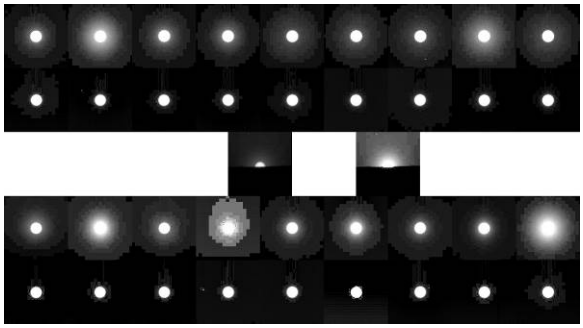

Figure 2. Solar images with blue filter. Each image is contrast stretched from 0 to 10% of the brightness of the Sun. The top row shows a sample of those images judged to show the feature while the Sun is above 18° elevation. The next row shows null images from the same elevation range. The 4th row shows icy images with the Sun below 18° elevation, and the bottom row shows similar null images. In the center are two version of one image (with 100% and 10% contrast stretches) showing the icy scattering is in the sky (beyond a low hill to the north), although that image was not used in the analysis.

Ice aerosol size:

For this report, all images at 451 nm have been analyzed. The short wavelength emphasizes the brightness of diffraction scattering for a given particle size. Dust is typically around r=1.5-1.6 μm, but may range from 1-2.5 μm [Smith, 2008]. Such particles have a forward-scattered diffraction peak within 10-20° from the Sun. The narrow angle scattering in the solar images is an order of magnitude closer to the Sun, and could represent diffraction by particles an order of magnitude larger. Such particles are assumed to be boundary layer water ice, given the temporal association with images of clouds [Moores *et al.,* 2010] and LIDAR profiles showing clouds in the boundary layer [Whiteway *et al.*, 2009].

First, a brightness profile for each image was created by finding the centroid of the Sun and calculating the average radiance within a series of concentric annuli as a function of distance. Figure 3 shows radiance profiles, normalized to the peak radiance of the image. The dynamic range of the 12-bit system, with less than saturated maximum radiance, is such that values of 0.001 are near the instrument floor (annulus-averaged results may be <0.001). Most images were within 1 DN of the background at 0.5° radius from the Sun's center. Profiles from these images were averaged for images with low and high Sun, and appear as the black lines in the figure. Brighter images were averaged into the blue curves. Typical 'icy' images fell to 1% of the Sun's brightness.

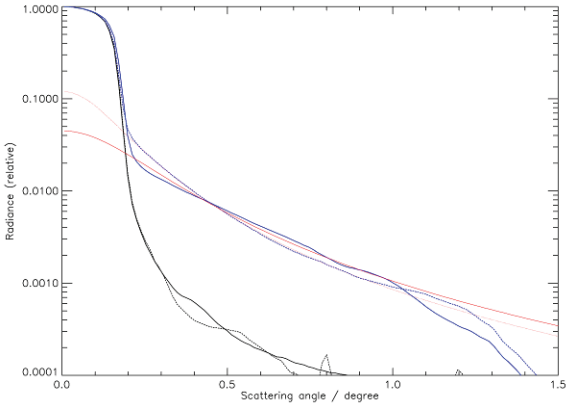

Figure 3. Radiance profile of solar images. The black solid and dashed lines are profiles of ice-free images, normalized to their peak brightness, for elevations above and below 18°, respectively. The blue solid and dashed lines are profiles of icy images (same elevation convention). The red solid and dotted lines are illustrative models of diffraction by 16- and 25- μm aerosols, using a variance of 0.5 for the size distribution.

For the averages, typical sizes can be estimated by assuming that all light more than 0.5° from the Sun is due to diffraction (for spatial variation) and a low, constant background. The red curves show the results, using r=16- and 25-μm aerosols, with a parameterized scattering function that uses real diffraction and (in this case) an arbitrary reflected and transmitted component of the phase function [Showalter *et al.,* 1992]. The smaller aerosols fit the mid-sol data; the larger aerosols fit the low-Sun data.

The process of fitting the radiance profiles can be repeated for each individual image, allowing the retrieval of ice aerosol size as well as ice optical depth. The optical depths resulting from such an exercise are shown in Fig. 1 (blue triangles). Sizes are shown in Fig. 4; in the morning hours, 30-μm aerosols are typical but the variation is more than a factor of two. In the afternoons, 10-16 μm aerosols are typical. The largest aerosols are seen near 3 AM, and are only seen in the middle of the mission. Ice aerosols were not detected in the first third of the mission, and the Sun was not up at 3 AM by the end of the mission (the first sunset/sunrise was sol 90).

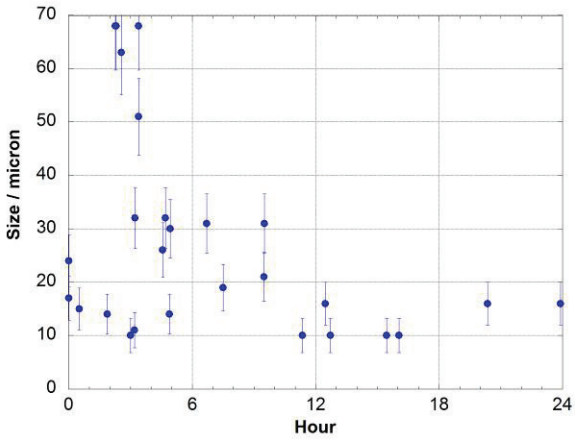

Figure 4. Retrieved ice aerosol radius. Uncertainties are currently somewhat notional, and are underestimated for the highest values.

Whiteway *et al.* 2009 report fall streaks in lidar profiles from the Phoenix lander; these are interpreted as ice crystals around 35 μm radius, and are seen at abundances of up to 1.9 precipitable microns of water. Our contemporaneous observation showed about 0.5 precipitable microns of ~26 μm particles.

For smaller ice aerosols, or for smaller ice loads, the near-Sun scattered light is not observable. Thus, the presence of smaller ice aerosols is not ruled out. Future work will include the analysis of data at all other available wavelengths and the tabulation of water ice abundance and size.

Conclusions:

Scattered light near the Sun varied with time, and was correlated with the time of the mission when ice clouds were visible in images and when the Phoenix Lidar saw clouds. The scattered light is above the instrument background, and corresponds to 10-70 μm aerosols. The largest aerosols are seen at the coldest time of sol. For data taken at about the same

time, these results are quantitatively similar to Lidar-based estimates. Sedimentation speeds at the (4-km) top of the day time boundary layer are ~7 km/sol, suggesting that the clouds are transient and transport water down to or within the boundary layer, possibly to the surface as snow.

Warmer modeled past climates are achievable when water ice clouds contain large particles [Urrata and Toon, 2013]. These observations demonstrate the presence of such clouds in certain (wet) environments on Mars today, and form a critical test for microphysical models applied to past climates.

References: Clancy *et al.* 2003, *J. Geophys. Res.*, **108**, E9, 5098. Daerden *et al.* 2010, *Geophys. Res. Lett.* **37**, L04203. Kahn, 1990, *J. Geophys. Res.* **95**, 14677-14693. Moores *et al*., 2010, *J. Geophys. Res.* **115**, E00E08. Showalter *et al*., 1992, *Icarus*, **100**, 394-411. Smith 2008, *Ann. Rev. Earth Planet. Sci*. **36**, 191-219. Smith and Lemmon, 1999, *J. Geophys. Res.*, **104**(E4), 8975–8985. Urrata and Toon, 2013, *Icarus* **226**, 229-250. Whiteway *et al*. 2009, *Science* **325**, 68-70.